Journal of Power Sources 348 (2017) 40–47

Contents lists available at ScienceDirect

Journal of Power Sources

journal homepage: www.elsevier.com/locate/jpowsour

Conformal bi-layered perovskite/spinel coating on a metallic wire network for solid oxide fuel cells *via* an electrodeposition-based route

Beom-Kyeong Park [a, b], Rak-Hyun Song [a], Seung-Bok Lee [a], Tak-Hyoung Lim [a], Seok-Joo Park [a], WooChul Jung [b], Jong-Won Lee [a, c, *]

[a] New and Renewable Energy Research Division, Korea Institute of Energy Research, 152 Gajeong-ro, Yuseong-gu, Daejeon, 34129, Republic of Korea
[b] Department of Materials Science and Engineering, Korea Advanced Institute of Science and Technology, 291 Daehak-ro, Yuseong-gu, Daejeon, 34141, Republic of Korea
[c] Department of Advanced Energy and Technology, Korea University of Science and Technology (UST), 217 Gajeong-ro, Yuseong-gu, Daejeon, 34113, Republic of Korea

HIGHLIGHTS

- Bi-layered perovskite/spinel oxide coating for solid oxide fuel cells.
- The bi-layered $LaMnO_3/Co_3O_4$ coating is fabricated *via* an electrodeposition route.
- The thin and dense coating is conformally formed on a metallic wire network.
- The coated wire network serves as an efficient current collector for tubular cells.

GRAPHICAL ABSTRACT

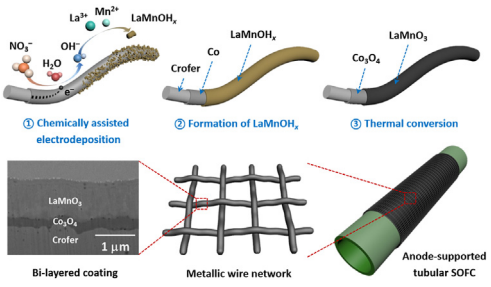

ARTICLE INFO

Article history:
Received 9 December 2016
Received in revised form
14 February 2017
Accepted 23 February 2017
Available online 2 March 2017

Keywords:
Solid oxide fuel cell
Bi-layered coating
Perovskite
Spinel
Electrodeposition

ABSTRACT

Solid oxide fuel cells (SOFCs) require low-cost metallic components for current collection from electrodes as well as electrical connection between unit cells; however, the degradation of their electrical properties and surface stability associated with high-temperature oxidation is of great concern. It is thus important to develop protective conducting oxide coatings capable of mitigating the degradation of metallic components under SOFC operating conditions. Here, we report a conformal bi-layered coating composed of perovskite and spinel oxides on a metallic wire network fabricated by a facile electrodeposition-based route. A highly dense, crack-free, and adhesive bi-layered $LaMnO_3/Co_3O_4$ coating of ~1.2 μm thickness is conformally formed on the surfaces of wires with ~100 μm diameter. We demonstrate that the bi-layered $LaMnO_3/Co_3O_4$ coating plays a key role in improving the power density and durability of a tubular SOFC by stabilizing the surface of the metallic wire network used as a cathode current collector. The electrodeposition-based technique presented in this study offers a low-cost and scalable process to fabricate conformal multi-layered coatings on various metallic structures.

1. Introduction

A solid oxide fuel cell (SOFC) is an electrochemical device that generates electricity from a fuel and an oxidant at high temperatures (600–800 °C) [1–3]. Over the years, SOFCs have received

* Corresponding author. New and Renewable Energy Research Division, Korea Institute of Energy Research, 152 Gajeong-ro, Yuseong-gu, Daejeon, 34129, Republic of Korea.
E-mail address: jjong277@kier.re.kr (J.-W. Lee).

http://dx.doi.org/10.1016/j.jpowsour.2017.02.080
0378-7753/

much attention owing to their advantages, including high conversion efficiency, fuel flexibility, and low emissions of toxic pollutants [2,4,5]. Various SOFC designs (*e.g.*, planar and tubular) have been devised to meet the requirements for specific applications, including desired electrochemical performance, durability, and reliability [6–8]. SOFCs require metallic components for current collection from electrodes and electrical connection between unit cells. For current collection of an anode-supported tubular cell, for example, a metallic wire coil or network (*e.g.*, mesh, felt, or foam) is wrapped around a cathode exposed to a high-temperature oxidizing atmosphere. The metallic component should maintain high electrical properties as well as intimate contact with the cathode during SOFC operation. Noble metals, such as Pt and Ag, have been used as cathode current collectors of tubular SOFCs [9–12]. In particular, Ag is preferred over other noble metals in terms of material cost; however, it becomes volatile at high temperatures, leading to a significant loss of its mass and structural integrity. Furthermore, mobile Ag species would migrate toward the cathode and form large-scale agglomerates and consequently reduce electrochemically active sites for oxygen reduction [12–14].

Fe–Cr-based alloys, such as Ducrolloy, Crofer 22 APU, AISI 430, and Inconel 600, are considered low-cost alternatives to Ag for SOFC applications. Metallic alloys mentioned above require protective conducting oxide coatings to mitigate degradation of their electrical performance and surface stability under high-temperature oxidizing conditions [15–25]. As demonstrated in many studies on metallic interconnects [15–25], a wide range of metal oxides can be used as protective coatings, for instance, rare-earth perovskites and Mn/Co-based spinels. Recently, many researchers have focused on a bi-layered coating comprising (*i*) a spinel oxide layer on a metallic substrate and (*ii*) a perovskite oxide layer on the spinel oxide [21–24]. Bloom Energy Co. demonstrated the efficacy and stability of a bi-layered $(La,Sr)MnO_3/Mn_{1.5}Co_{1.5}O_4$ coating on the metallic interconnect during long-term performance tests [22]. Our group reported that a bi-layered $LaCoO_3/Co_3O_4$ coating effectively mitigates degradation of the electrical properties of the Crofer interconnect [24]. The bi-layered perovskite/spinel coating is believed to reduce the degradation of stainless steels in the following ways: (*i*) the spinel oxide layer suppresses oxygen diffusion toward the metallic substrate and thus inhibits the growth of Cr oxide scales with poor conductivity; and (*ii*) the perovskite layer acts as another barrier to the transport of Cr (solid-state and/or gas phase) and oxygen [21,22,24]. In addition, a highly conductive perovskite oxide layer plays a beneficial role in facilitating electronic conduction between the cathode and the protective coating [23,24].

In this study, we report a conformal bi-layered perovskite/spinel coating on a metallic wire network fabricated by a facile electrodeposition-based route. A bi-layered $LaMnO_3/Co_3O_4$ coating is fabricated by a three-step process: (*i*) electrodeposition of metallic Co; (*ii*) chemically assisted electrodeposition of $LaMnOH_x$; and (*iii*) thermal conversion of $LaMnOH_x$/Co to $LaMnO_3/Co_3O_4$. In our previous study, an electrodeposition-based approach was used to fabricate a bi-layered $LaCoO_3/Co_3O_4$ coating on a Crofer plate for applications in SOFC interconnects [24]. In this work, the process is modified to synthesize phase-pure $LaMnO_3$ that is known to have lower ionic conductivity (oxygen permeability) than $LaCoO_3$ and thus to prevent more effectively the oxygen inward diffusion [26–28]. For applications to cathode current collectors for anode-supported tubular cells, moreover, a conformal $LaMnO_3/Co_3O_4$ coating is fabricated on a stainless steel wire network (Crofer mesh) with a complicated shape and is shown to serve as an effective protective layer, leading to improved power density and durability of the cell.

2. Experimental

2.1. Preparation of a bi-layered perovskite/spinel coating

A rectangular Crofer 22 APU mesh (ThyssenKrupp) with dimensions of 5 mm × 20 mm (real surface area = 1.75 cm^2) was used as a metallic wire network. For the electrodeposition of metallic Co, the Crofer and Pt meshes were employed as the working and counter electrodes, respectively. The electrolyte solution was prepared by dissolving 0.25 M $CoCl_2 \cdot 6H_2O$ (98%, Aldrich), 0.25 M $CoSO_4 \cdot H_2O$ (≥99.0%, Aldrich), and 0.1 M H_3BO_3 (99.5%, Samchun Pure Chemical) in deionized water. The solution pH was adjusted to 3.3 by adding 0.1 M HCl. The metallic Co layer was electrodeposited at a cathodic current density of 28 mA cm^{-2} for 20 s. The electrodeposition of $LaMnOH_x$ was performed using an electrochemical cell composed of cathodic and anodic chambers. The cathodic chamber contained a Co/Crofer mesh (working electrode), an Ag/AgCl reference electrode (with saturated NaCl), and a mixed metal nitrate solution of $La(NO_3)_3 \cdot 6H_2O$ (99.99%, Kanto) and $Mn(NO_3)_2 \cdot 4H_2O$ (≥97.0%, Aldrich) in deionized water. To find the optimum solution composition for the synthesis of phase-pure $LaMnO_3$, the Mn^{2+} concentration ($[Mn^{2+}]$) was varied between 20 and 180 mM, while the La^{3+} concentration ($[La^{3+}]$) was fixed at 20 mM. The pH value of the metal nitrate solution was adjusted to 4.5 by adding 0.1 M HCl. A Crofer plate with dimensions of 10 mm × 10 mm × 1 mm was used for the optimization study on the synthetic conditions of $LaMnO_3$ films. The anodic chamber contained a Pt mesh (counter electrode) and a KNO_3 solution (≥99.0%, Aldrich) that has the same concentration as the metal nitrate solution in the cathodic chamber. Two chambers were divided by an anion-exchange membrane (APS4, Asahi Glass) to prevent unintended reactions (*e.g.*, anodic oxidation of metal ions) on the Pt counter electrode. Electrodeposition was carried out at a cathodic current density of 0.5 mA cm^{-2} for 20 min. After drying at 70 °C, the $LaMnOH_x$/Co/Crofer mesh was heat-treated in air at 800 °C for 2 h to fabricate $LaMnO_3/Co_3O_4$/Crofer.

2.2. Material characterization

The crystal structure and phases were analyzed by X-ray diffraction (XRD, 2500 D/MAX, Rigaku) with Cu K_α (λ = 1.5405 Å) radiation. The surface morphologies were observed by scanning electron microscopy (SEM, Hitachi SU–8230). A focused ion beam (FIB) equipped with a SEM (FEI Helios Nanolab 450 F1) was used to perform the cross-sectional observations of the coatings. The surface chemistry was examined by X-ray photoelectron spectroscopy (XPS, Thermo MultiLab 2000 spectrometer) combined with energy dispersive X-ray spectroscopy (EDS, Ametek). The fraction of Mn^{4+} in $LaMnO_3$ was measured by a well-known chemical method involving redox titration [29]. The $LaMnO_3$ deposit was dissolved in a mixed solution containing 5 M H_2SO_4 and 0.01 mM $Na_2C_2O_4$. After this, 0.2 M $KMnO_4$ was added slowly dropwise to the mixed solution until the pink color appeared. The fraction of Mn^{4+} was estimated from the amount of $Na_2C_2O_4$ that had been used to reduce Mn^{3+} and Mn^{4+} to Mn^{2+}. The chemical compositions were determined using an inductively coupled plasma mass spectrometer (ICP–MS, Aglient). For the titration and ICP–MS analyses, a Pt mesh was used as a substrate to precisely determine the compositions without complications arising from Crofer.

2.3. Performance evaluation of SOFCs

To evaluate the feasibility of the $LaMnO_3/Co_3O_4$/Crofer mesh as a cathode current collector for SOFCs, an anode-supported tubular cell was fabricated as reported elsewhere [30]. The tubular cell

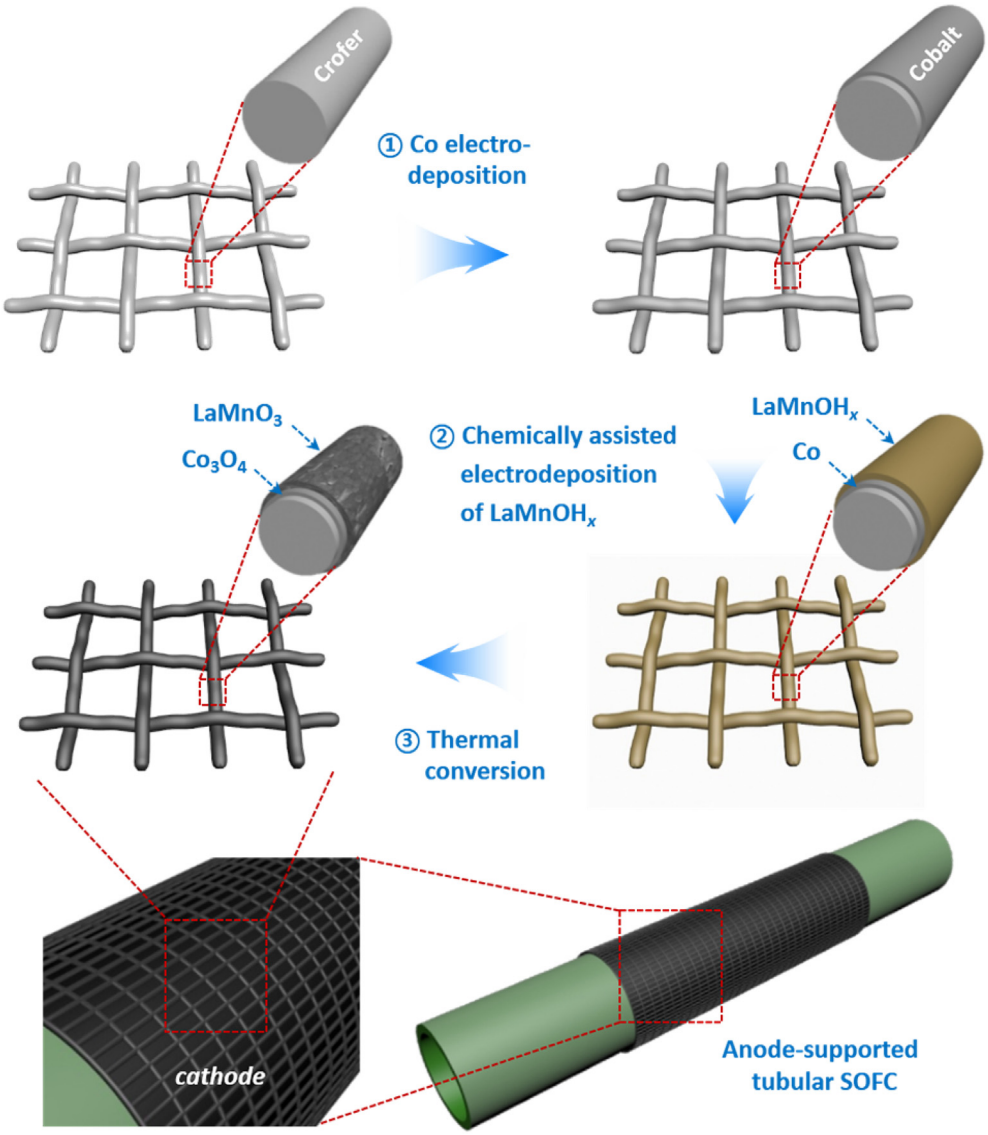

Fig. 1. Schematic diagram of the fabrication process of a bi-layered perovskite/spinel ($LaMnO_3/Co_3O_4$) coating on a metallic (Crofer) wire network.

consisted of $La_{0.6}Sr_{0.4}Co_{0.2}Fe_{0.8}O_3$ (LSCF) (cathode current collecting layer), $(La_{0.85}Sr_{0.15})_{0.9}MnO_3$ (LSM)–8 mol.% Y_2O_3-stabilized ZrO_2 (YSZ) (cathode functional layer), YSZ (electrolyte), and NiO–YSZ (anode functional layer and support) (Ni–YSZ upon reduction) (see Fig. S1 in the Supplementary Data). Metal tubes were attached to the cell using a ceramic adhesive to supply H_2 into the anode support. For current collection, the $LaMnO_3/Co_3O_4$/Crofer mesh was wrapped around the LSCF cathode using an $La_{0.6}Sr_{0.4}CoO_3$ paste, while an Ni mesh was inserted into the anode support and attached onto the surface of NiO–YSZ using an Ni paste. The $La_{0.6}Sr_{0.4}CoO_3$ and Ni pastes were used to ensure the intimate contact between the electrodes and the current collectors, thereby reducing the contact resistances [31,32]. The polarization curve of the cell was obtained at 800 °C, and then ac-impedance spectra were periodically measured every 50 h at open-circuit voltages (OCVs). The impedance measurements were carried out using a Bio-Logic SP–240 with an ac signal of 10 mV amplitude. During electrochemical testing, the anode and cathode were fed with H_2 gas humidified with 3 vol% H_2O and air, respectively. In addition, a thermal cycling experiment of the $LaMnO_3/Co_3O_4$/Crofer mesh was conducted between 200 and 900 °C at a ramp rate of 3 °C min^{-1}.

3. Results and discussion

Fig. 1 presents a schematic diagram of the fabrication process of a bi-layered perovskite/spinel coating on a metallic (Crofer) wire network. The bi-layered coating is composed of a Co_3O_4 spinel layer on the metallic substrate and an $LaMnO_3$ perovskite layer on the Co_3O_4 layer, and it was fabricated by a three-step process involving (*i*) Co electrodeposition, (*ii*) electrodeposition of a mixed metal hydroxide ($LaMnOH_x$), and (*iii*) thermal conversion of $LaMnOH_x$/Co to $LaMnO_3/Co_3O_4$.

In step (*ii*), $LaMnOH_x$ was synthesized on a Co/Crofer wire network *via* chemically assisted electrodeposition as follows [24,33,34]: upon the cathodic polarization of the working electrode (Co/Crofer) in the mixed metal nitrate bath, nitrate ions (NO_3^-) are electrochemically reduced to hydroxide ions (OH^-), which leads to a local increase of pH near the working electrode and subsequently the chemical precipitation of $LaMnOH_x$. A typical potential *vs.* time profile recorded during $LaMnOH_x$ electrodeposition is presented in Fig. 2(a). Note that a bare Crofer plate (without electrodeposited Co) was used to demonstrate the hydroxide formation. The measured potentials are much higher than the reduction potentials of La^{3+}

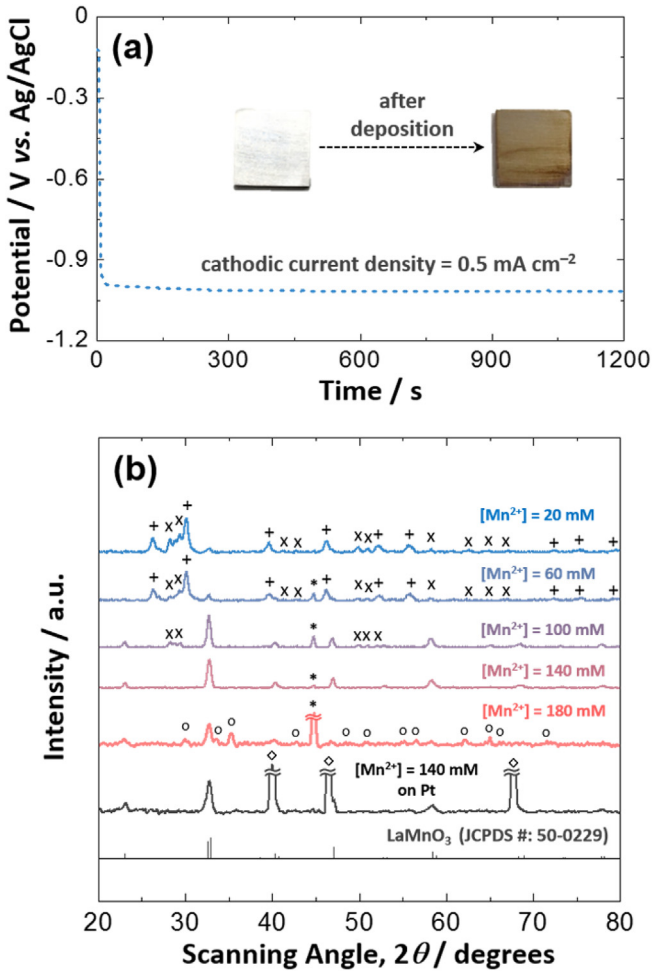

Fig. 2. (a) Potential *vs.* time profile measured during the chemically assisted electrodeposition of $LaMnOH_x$ at a cathodic current density of 0.5 mA cm^{-2} and photographs of the bare and $LaMnOH_x$-coated Crofer plates. (b) XRD patterns of $LaMnOH_x$ films heat-treated in air at 800 °C. Electrodeposition was performed from mixed nitrate solutions with various compositions: $[La^{3+}]$ = 20 mM and $[Mn^{2+}]$ = 20–180 mM. Symbols '+', '×', '○', and '•' indicate La_2O_3, La_2CrO_6, Mn_3O_4, and Crofer, respectively.

(−2.58 V *vs.* Ag/AgCl) and Mn^{2+} (−1.39 V *vs.* Ag/AgCl), which indicates that La^{3+} and Mn^{2+} would not be electrochemically reduced to their metal phases. After electrodeposition, a white-brown deposit of $LaMnOH_x$ was formed on the Crofer substrate, as shown in Fig. 2(a). Here, it should be pointed out that the processing parameters used for step (*ii*) are different from those for step (*i*). In general, the electrodeposition process of metallic Co proceeds *via* direct reduction of Co^{2+} to Co, and thus, it can be conducted at a relatively high current density [35]. On the other hand, the chemically assisted electrodeposition of $LaMnOH_x$ requires a relatively low current density to produce a dense, crack-free, and adhesive layer. At high cathodic currents, the rate of NO_3^- reduction (OH^- generation) would become much faster than that of $LaMnOH_x$ precipitation, which causes the excessive growth of the high pH region and results in the formation of deposits with low density and poor adhesion strength [24].

To find the optimum solution composition for the fabrication of single-phase $LaMnO_3$, electrodeposition was performed on bare Crofer plates from mixed metal nitrate solutions having various compositions; $[Mn^{2+}]$ was changed between 20 and 180 mM, while $[La^{3+}]$ was fixed at 20 mM. A bare Crofer plate was used as a substrate to clearly analyze the XRD data of the heat-treated $LaMnOH_x$ deposit. A Co/Crofer wire network was found to add complications to the analysis: (*i*) Co_3O_4 and Mn_3O_4 show similar diffraction patterns, and (*ii*) the XRD data obtained from the mesh-type specimens exhibit relatively low signal-to-noise ratios. Fig. 2(b) exhibits the XRD patterns of the hydroxide deposits heat-treated in air at 800 °C. The film fabricated with $[Mn^{2+}] = 20$ mM was composed of $LaMnO_3$ and secondary phases of La_2O_3 and La_2CrO_6 (denoted by symbols '+' and '×', respectively). The amount of the secondary phases decreased with increasing $[Mn^{2+}]$ from 20 to 140 mM, and phase-pure $LaMnO_3$ was synthesized with $[Mn^{2+}]$ = 140 mM. Given that the solubility product constants of $La(OH)_3$ and $Mn(OH)_2$ are ~2.0×10^{-19} and ~1.9×10^{-13}, respectively [36,37], the yield of $Mn(OH)_2$ precipitation would be lower than that of $La(OH)_3$ during electrodeposition, and thus $[Mn^{2+}]$ should be higher than $[La^{3+}]$. At $[Mn^{2+}]$ = 180 mM; however, Mn_3O_4 (denoted by symbol 'o') was detected as the secondary phase. The XRD patterns of the $LaMnO_3$ films synthesized with the optimized composition on both Crofer and Pt substrates clearly show a rhombohedral perovskite structure (JCPDS No. 50-0229) without any secondary phases.

Based on the optimization study presented above, a $LaMnOH_x$ film was formed on a Co/Crofer wire network and then heat-treated in air at 800 °C to fabricate a bi-layered $LaMnO_3/Co_3O_4$ coating. The XRD pattern of the bi-layered coating in Fig. 3(a) clearly shows characteristic peaks for both $LaMnO_3$ and Co_3O_4 (denoted by symbols '◆' and '▼', respectively). Due to the complicated shape (rounded surfaces and bent wires) and small exposed area of the mesh-type specimen, the XRD pattern in Fig. 3(a) exhibits a low signal-to-noise ratio, which makes some diffraction peaks invisible. It should be noted, however, that the XRD patterns of $LaMnO_3$ on the Crofer and Pt plates (Fig. 2(b)) clearly show all of the characteristic peaks corresponding to $LaMnO_3$. An XPS analysis was employed to acquire further information on the surface chemistry of the bi-layered coating, as presented in Fig. 3(b). The O 1s spectrum shows two peaks at binding energies (BEs) of 528.8 and 531.3 eV, which are assigned to the lattice oxygen (O^{2-}) and absorbed oxygen species (O-, O_2^-, or O_2^{2-}), respectively [39,40]. The Mn 2p spectrum exhibits a spin-orbit doublet for Mn $2p_{3/2}$ and Mn $2p_{1/2}$. The asymmetry of the two peaks implies the coexistence of Mn^{3+} and Mn^{4+} on the $LaMnO_3$ surface; namely, the peaks at BE = 641.1 eV and 642.9 eV are assigned to Mn^{3+} and Mn^{4+}, respectively. The observed Mn 2p spectrum is in good agreement with the XPS data of $LaMnO_3$ in the literature [38–41]. Under an oxidizing atmosphere, $LaMnO_3$ is known to have oxygen excess, which is accompanied by the oxidation of Mn^{3+} to Mn^{4+} ions for charge compensation [42]. In Fig. 3(b), the fraction of Mn^{4+} was estimated to be ~0.28 from the deconvolution analysis, similar to the value obtained from the titration method (~0.3) and the data reported by Tofield et al. [43]. The La 3d spectrum shows La $3d_{5/2}$ and La $3d_{3/2}$ spin-orbit doublet peaks that have a double peak structure (BE = 833.9 and 837.9 eV for La $3d_{5/2}$ and BE = 850.7 and 854.7 eV for La $3d_{3/2}$) due to electron transfer from the oxygen valence band to the empty La 4f level [44]. In addition, compositional analyses were performed using EDS, XPS, and ICP–MS, and the ratio of La/Mn was estimated to be ~0.96 (EDS), ~0.91 (XPS), and ~0.90 (ICP–MS).

Fig. 4(a)–(c) show the surface morphologies of the bare Crofer, Co/Crofer, and $LaMnO_3/Co_3O_4$/Crofer wires, respectively. It is seen that the bare Crofer wire of ~100 μm diameter has a clean metallic surface without showing any characteristic crystalline morphology (Fig. 4(a)), and the dense Co film was conformally deposited onto the Crofer wire (Fig. 4(b)). The SEM micrographs in Fig. 4(c) indicate that the $LaMnO_3/Co_3O_4$/Crofer wire has a conformal, dense, and crack-free surface with nano-sized and polygonal-shaped grains, which can serve as an effective protective coating. For cross-sectional observation, the coated Crofer wire was sputtered with

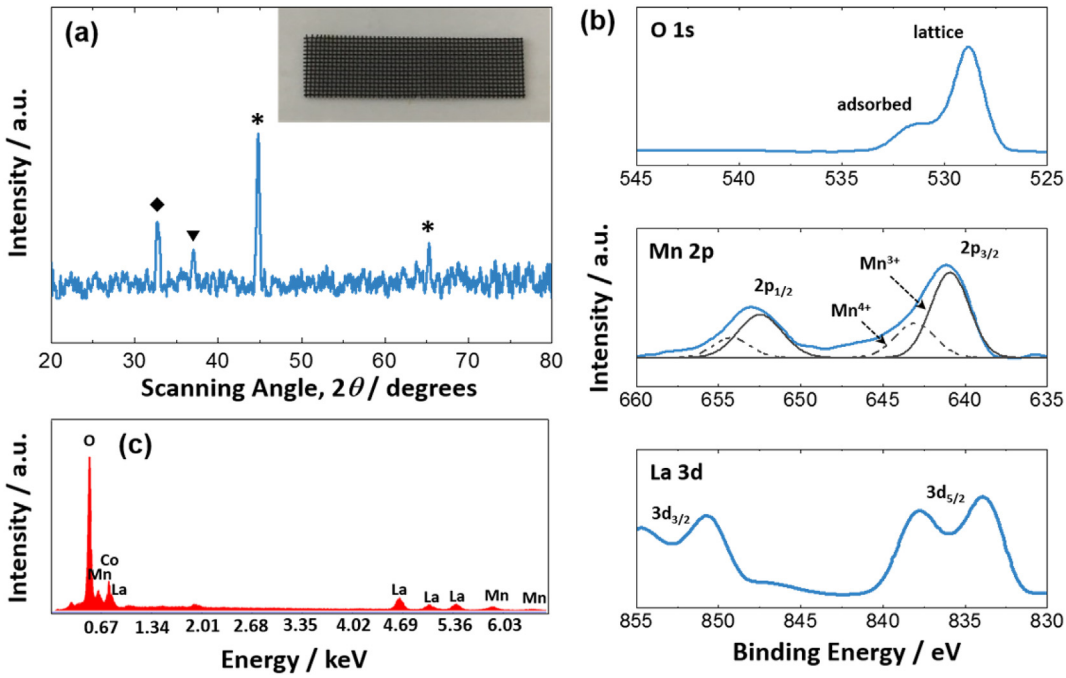

Fig. 3. (a) XRD pattern and photograph of the $LaMnO_3/Co_3O_4$/Crofer wire network. Symbols '◆', '▼', and '*' indicate $LaMnO_3$, Co_3O_4, and Crofer, respectively. (b) XPS spectra of the O 1s, Mn 2p, and La 3d regions, and (c) EDS spectrum obtained for the $LaMnO_3/Co_3O_4$ coating.

a protective Pt layer and was then dissected using an FIB technique. Fig. 4(d) and (e) present cross-sectional SEM images of the Co_3O_4/Crofer and $LaMnO_3/Co_3O_4$/Crofer wires, respectively. From a comparison of the two micrographs, we confirm the formation of the bi-layered $LaMnO_3/Co_3O_4$ on the Crofer wire. No connected pores are detected across the thickness of the bi-layered coating, and the interfaces between the layers are cohesive without any cracks or delamination. The thicknesses of Co_3O_4 and $LaMnO_3$ were estimated to be ~250 nm and ~1 μm, respectively, which are much smaller in comparison to coatings prepared by powder-sintering techniques [15,16,19–23]. The structural and chemical analyses reveal that the bi-layered ($LaMnO_3/Co_3O_4$) coating was successfully fabricated onto the Crofer wire network through the electrodeposition process combined with thermal conversion. The fabrication method presented in this study offers the following advantages over conventional techniques. First, thin and dense coatings made of perovskite and spinel oxides can be conformally formed on porous substrates with complicated shapes. During the chemically assisted electrodeposition process, the electrochemical reduction of NO_3^- to OH^- occurs on any surfaces of the conductive metallic wires exposed to the solution, leading to the formation of a uniform and conformal $LaMnOH_x$ layer ($LaMnO_3$ after thermal conversion). Second, the electrodeposition-based approach provides a simple, low-cost, and scalable process without the need for powder synthesis/calcination, slurry preparation/coating, and high-temperature sintering (>800 °C).

We employed the $LaMnO_3/Co_3O_4$/Crofer wire network as a cathode current collector and evaluated its feasibility in an anode-supported tubular SOFC. The cell was held at 800 °C for 100 h prior to electrochemical polarization measurements. Fig. 5(a) compares the polarization (voltage *vs.* current) curves of the tubular cells measured at 800 °C using the bare Crofer and $LaMnO_3/Co_3O_4$/Crofer wire networks. The OCV values of both cells were measured to be ~1.1 V, indicating that there was no fuel leakage from the cell. On the other hand, the maximum power density of the cell assembled with $LaMnO_3/Co_3O_4$/Crofer was estimated to be 460 mW cm^{-2}, which was higher than that of the cell with bare Crofer. To gain in-depth insight into the difference in the cell performance, electrochemical impedance spectroscopy was carried out, and the results are shown in Fig. 5(b). The measured impedance spectra were composed of two depressed, slightly overlapping arcs. The high-frequency intercept corresponds to the ohmic resistance arising from the electrode, electrolyte, and current collector [45–48]. The high-frequency arc is attributed to the electrochemical reactions at the electrode/electrolyte interfaces, whereas the low-frequency arc is largely due to the mass transport in the anode support [45–48]. Of particular note is the lower ohmic resistance of the cell with $LaMnO_3/Co_3O_4$/Crofer compared to that of the cell with bare Crofer. Keeping in mind that bare Crofer is quite susceptible to oxidation and would have been passivated by Cr_2O_3 scales during the conditioning step for 100 h, this result demonstrates the beneficial role of the bi-layered $LaMnO_3/Co_3O_4$ coating in improving the surface stability of Crofer.

To evaluate the long-term stability of the cathode current collectors, the evolution of the impedance spectra was monitored over 1000 h of continuous testing. The data were also measured on the cell using a benchmark current collector (Ag mesh). Fig. 6(a)–(c) present the variations of the impedance spectra with time obtained using the bare Crofer, $LaMnO_3/Co_3O_4$/Crofer, and Ag wire networks, respectively. During the long-term test, the cell with bare Crofer exhibits a more significant increase of the ohmic resistance in comparison to Ag and $LaMnO_3/Co_3O_4$/Crofer. The variations of ohmic resistances for different current collectors are plotted against time in Fig. 6. The ohmic resistance of the cell with bare Crofer increased by more than 60% over 1000 h, which implies severe degradation of the electrical properties. On the other hand, the ohmic resistance of the cell with $LaMnO_3/Co_3O_4$/Crofer remained almost constant, as in the case of Ag. The polarization

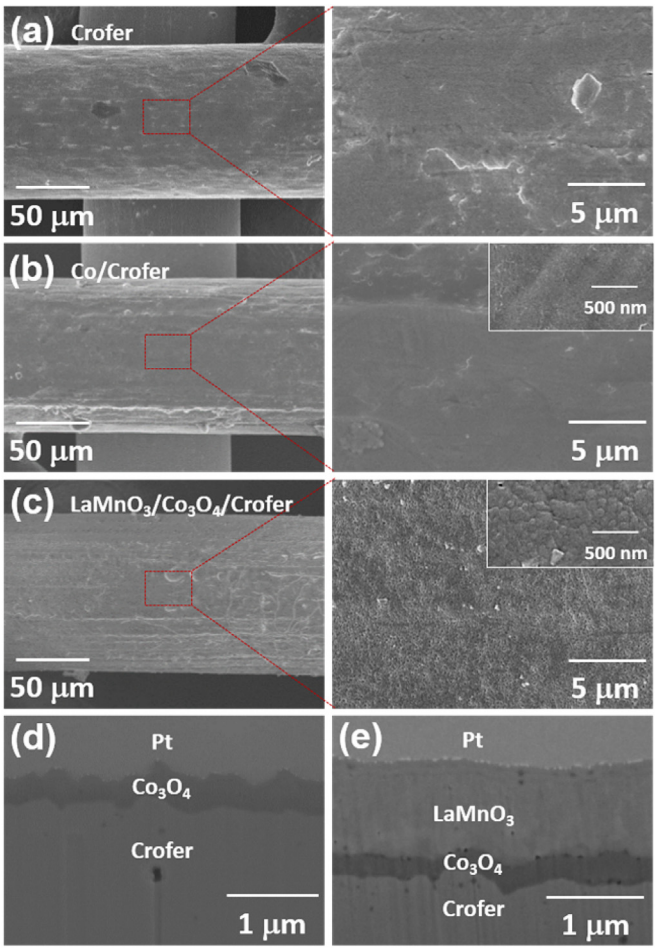

Fig. 4. SEM micrographs of the (a) bare Crofer, (b) Co/Crofer, and (c) $LaMnO_3/Co_3O_4$/Crofer wires. Cross-sectional SEM images of the Co_3O_4/Crofer and $LaMnO_3/Co_3O_4$/Crofer wires are presented in (d) and (e), respectively. The cross-sectional images are tilted 52° to the vertical so that the scale bars are trigonometrically corrected.

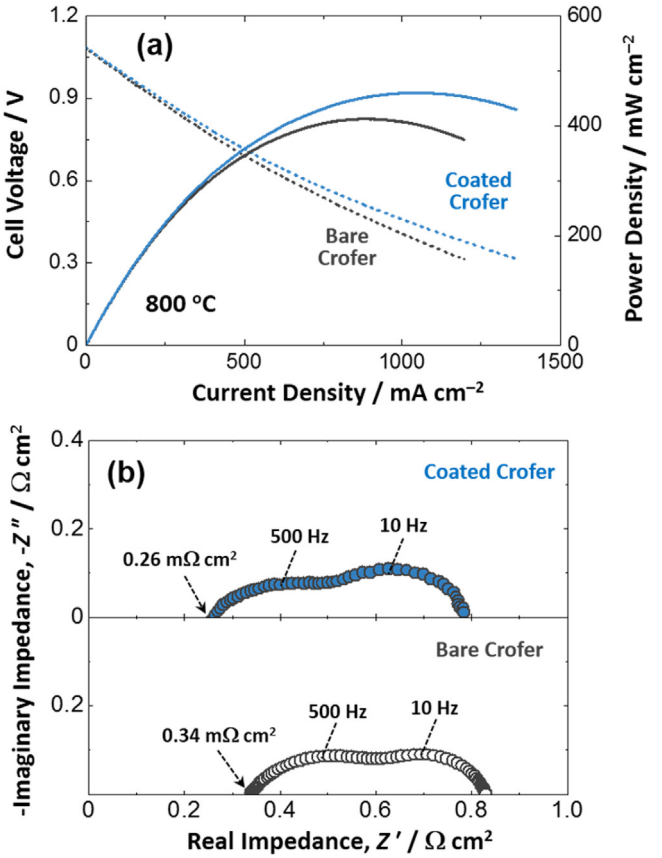

Fig. 5. (a) Polarization (voltage *vs.* current) curves and (b) impedance spectra of the anode-supported tubular SOFCs measured at 800 °C using the bare Crofer and $LaMnO_3/Co_3O_4$/Crofer wire networks.

curves measured after 1000 h of continuous testing (Fig. S2) further confirm that $LaMnO_3/Co_3O_4$/Crofer leads to considerably improved durability of the cell, as compared with bare Crofer. At this point, it is of interest to compare the stability of the Crofer wire networks coated with Co_3O_4, $LaMnO_3$, and $LaMnO_3/Co_3O_4$ and to prove the efficacy of the bi-layered perovskite/spinel coating. For this purpose, we conducted accelerated oxidation tests in air at 950 °C. The weight gains and SEM micrographs of the oxidized samples are presented in Fig. S3. The $LaMnO_3/Co_3O_4$/Crofer wire network showed a much lower weight increase (~0.6 mg cm^{-2}) after 200 h, compared with Co_3O_4/Crofer (~1.9 mg cm^{-2}) and $LaMnO_3$/Crofer (~3.2 mg cm^{-2}), indicating improved stability against high-temperature oxidation. Furthermore, no significant change in the surface morphology of $LaMnO_3$ was observed.

The current collector should endure repeated thermal cycles during SOFC operation. The stabilities of Ag and $LaMnO_3/Co_3O_4$/Crofer were examined and compared during thermal cycling between 200 and 900 °C. From the photographs and micrographs of pristine and cycled Ag in Fig. 7(a) and (b), it is seen that Ag slightly melted, leaving a dark stain on the zirconia substrate, after 10 thermal cycles. Moreover, morphological changes due to Ag evaporation, such as faceting or striation, are visible on the Ag wire. On the other hand, $LaMnO_3/Co_3O_4$/Crofer shows high structural stability without any signs of cracking or delamination. This demonstrates the thermal compatibility of the bi-layered $LaMnO_3/Co_3O_4$ coating with the Crofer substrate, as expected from the coefficients of thermal expansion of $LaMnO_3$ (~12 × 10^{-6} K^{-1}) [49], Co-based spinel (~10 × 10^{-6} K^{-1}) [23], and Crofer (~12 × 10^{-6} K^{-1}) [50]. The thermal cycling caused grain growth of $LaMnO_3$; however, this might not have a significant effect on the stability of the bi-layered coating. These results strongly suggest that $LaMnO_3/Co_3O_4$/Crofer can serve as an effective cathode current collector with high stability under SOFC operating conditions.

4. Conclusions

In this study, a conformal bi-layered perovskite/spinel coating comprising $LaMnO_3$ and Co_3O_4 was fabricated on a metallic wire network by a facile electrodeposition-based route: (*i*) Co electrodeposition, (*ii*) electrodeposition of $LaMnOH_x$, and (*iii*) thermal conversion of $LaMnOH_x$/Co to $LaMnO_3/Co_3O_4$. The fabrication method proposed here provides attractive features over conventional coating techniques based on powder sintering: (*i*) a thin and dense bi-layered $LaMnO_3/Co_3O_4$ coating of ~1.2 μm thickness can be conformally formed on the Crofer wire network; and (*ii*) the electrodeposition approach provides a simple, low-cost, and scalable process without the need for complicated procedures, *i.e.*, powder synthesis/calcination, slurry preparation/coating, and high-temperature sintering. When applied to a cathode current collector for anode-supported tubular SOFCs, the bi-layered $LaMnO_3/Co_3O_4$ coating acts as an effective protective layer to inhibit the high-temperature oxidation of the Crofer wire surface, thereby

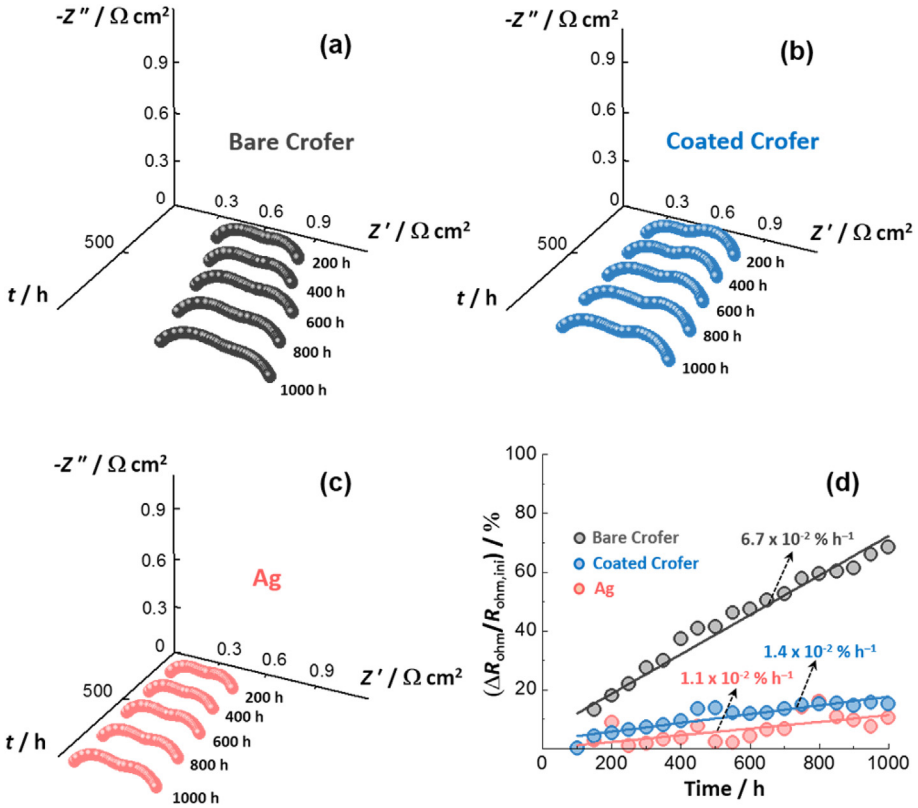

Fig. 6. Impedance spectra of the anode-supported tubular SOFCs with the (a) bare Crofer, (b) $LaMnO_3/Co_3O_4$/Crofer, and (c) Ag wire networks measured during continuous testing at 800 °C. (d) Increases of the ohmic resistance (ΔR_{ohm}) relative to the initial value ($R_{ohm,ini}$) with time measured for different current collectors.

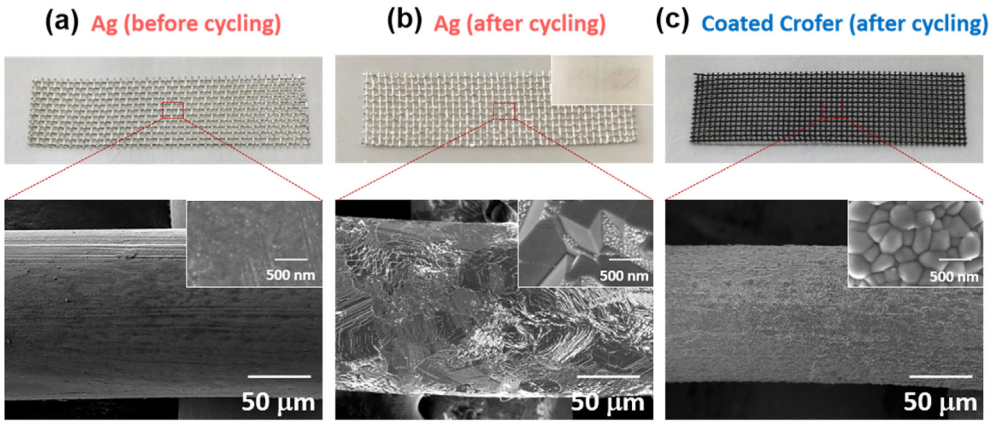

Fig. 7. Photographs and SEM micrographs of (a) pristine Ag and (b) thermally cycled Ag, and (c) thermally cycled $LaMnO_3/Co_3O_4$/Crofer wire networks. Thermal cycling was conducted between 200 and 900 °C at a ramp rate of 3 °C min^{-1}.

improving the power density and durability of the cell. Furthermore, $LaMnO_3/Co_3O_4$/Crofer shows high structural stability without cracking or delamination over the course of repeated thermal cycles.

Acknowledgements

This work was supported by the Materials Technology Development Program (Phase II) (KEIT Project No. 10051003) and the International Collaborative Energy Technology R&D Program (KETEP Project No. 10051003), which were funded by the Ministry of Trade, Industry & Energy, Republic of Korea.

Appendix A. Supplementary data

Supplementary data related to this article can be found at http://dx.doi.org/10.1016/j.jpowsour.2017.02.080.

References

[1] E.D. Wachsman, K.-T. Lee, Lowering the temperature of solid oxide fuel cells, Science 334 (2011) 935–939.
[2] A. Choudhury, H. Chandra, A. Arora, Application of solid oxide fuel cell technology for power generation—A review, Renew. Sustain. Energy Rev. 20 (2013) 430–442.
[3] N. Mahato, A. Banerjee, A. Gupta, S. Omar, K. Balani, Progress in material section for solid oxide fuel cell technology: a review, Prog. Mater. Sci. 72

(2015) 141–337.
[4] C. Strazza, A.D. Borghi, P. Costamagna, A. Traverso, M. Santin, Comparative LCA of methanol-fuelled SOFCs as auxiliary power systems on-board ships 87 (2010) 1670–1678.
[5] P. Kazempoor, V. Dorer, A. Weber, Modeling and evaluation of building integrated SOFC systems, Int. J. Hydrogen Energy 36 (2011) 13241–13249.
[6] S.C. Singhal, Advances in solid oxide fuel cell technology, Solid State Ion. 135 (2000) 305–313.
[7] N.Q. Minh, Solid oxide fuel cell technology–features and applications, Solid State Ion. 174 (2004) 271–277.
[8] C. Bao, N. Cai, E. Croiset, An analytical model of view factors for radiation heat transfer in planar and tubular solid oxide fuel cells, J. Power Sources 196 (2011) 3223–3232.
[9] N. Akhtar, S.P. Decent, K. Kendall, Structural stability of silver under single-chamber solid oxide fuel cell conditions, Int. J. Hydrogen Energy 34 (2009) 7807–7810.
[10] K.C.R.D. Silva, B.J. Kaseman, D.J. Bayless, Silver (Ag) as anode and cathode current collectors in high temperature planar solid oxide fuel cells, Int. J. Hydrogen Energy 36 (2011) 779–786.
[11] Y. Chen, F. Wang, D. Chen, F. Dong, H.-J. Park, C. Kwak, Z. Shao, Role of silver current collector on the operational stability of selected cobalt-containing oxide electrodes for oxygen reduction reaction, J. Power Sources 210 (2012) 146–153.
[12] Y. Gong, C. Qin, K. Huang, Can silver be a reliable current collector for electrochemical tests? ECS Electrochem. Lett. 2 (2013) F4–F7.
[13] T.Z. Sholklapper, V. Radmilovic, C.P. Jacobson, S.J. Visco, L.C.D. Jonghe, Nanocomposite Ag–LSM solid oxide fuel cell electrodes, J. Power Sources 175 (2008) 206–210.
[14] G.-H. Zhou, X.-Z. Fu, J.-L. Luo, K.T. Chuang, A.R. Sanger, Ag modified LSCF as cathode material for protonic conducting SOFCs, Mater. Technol. 28 (2013) 3–8.
[15] Z. Yang, G.-G. Xia, G.D. Maupin, J.W. Stevenson, Evaluation of perovskite overlay coatings on ferritic stainless steels for SOFC interconnect applications, J. Electrochem. Soc. 153 (2006) A1852–A1858.
[16] M.-J. Tsai, C.-L. Chu, S. Lee, $La_{0.6}Sr_{0.4}Co_{0.2}Fe_{0.8}O_3$ protective coatings for solid oxide fuel cell interconnect deposited by screen printing, J. Alloy. Compd. 489 (2010) 576–581.
[17] J. Wu, X. Liu, Recent development of SOFC metallic interconnect, J. Mater. Sci. Technol. 26 (2010) 293–305.
[18] N. Shaigan, W. Qu, D.G. Ivey, W. Chen, A review of recent progress in coatings, surface modifications and alloy developments for solid oxide fuel cell ferritic stainless steel interconnects, J. Power Sources 195 (2010) 1529–1542.
[19] Z.J. Feng, C.L. Zeng, $LaCrO_3$-based coatings deposited by high-energy micro-arc alloying process on a ferritic stainless steel interconnect material, J. Power Sources 195 (2010) 4242–4246.
[20] Y. Fang, C. Wu, X. Duan, S. Wang, Y. Chen, High-temperature oxidation process analysis of $MnCo_2O_4$ coating on Fe–21Cr alloy, Int. J. Hydrogen Energy 36 (2011) 5611–5616.
[21] M. Palcut, L. Mikkelsen, K. Neufeld, M. Chen, R. Knibbe, P.V. Hendriksen, Efficient dual layer interconnect coating for high temperature electrochemical devices, Int. J. Hydrogen Energy 37 (2012) 14501–14510.
[22] J. Wilson, M. Pillai, T. Armstrong, U.S. Patent 20130230792A1, 2013.
[23] X. Yang, H. Tu, Q. Yu, Fabrication of Co_3O_4 and $La_{0.6}Sr_{0.4}CoO_{3-\delta}$–$Ce_{0.8}Gd_{0.2}O_{2-\delta}$ dual layer coatings on SUS430 steel by in-situ phase formation for solid oxide fuel cell interconnects, Int. J. Hydrogen Energy 40 (2015) 607–614.
[24] B.-K. Park, R.-H. Song, S.-B. Lee, T.-H. Lim, S.-J. Park, C.-O. Park, J.-W. Lee, A perovskite-type lanthanum cobaltite thin film synthesized via an electrochemical route and its application in SOFC interconnects, J. Electrochem. Soc. 162 (2015) F1549–F1554.
[25] G. Chen, X. Xin, T. Luo, L. Liu, Y. Zhou, C. Yuan, C. Lin, Z. Zhan, S. Wang, $Mn_{1.4}Co_{1.4}Cu_{0.2}O_4$ spinel protective coating on ferritic stainless steels for solid oxide fuel cell interconnect applications, J. Power Sources 278 (2015) 230–234.
[26] N.Q. Minh, T. Takahashi, Science and Technology of Ceramic Fuel Cells, Elsevier, Amsterdam, 1995.
[27] O.I. Klyushnikov, V.V. Sal'nikov, N.M. Bogdanovich, X-ray photoelectron spectra of $La_{0.7}Ca_{0.3}MnO_3$ and $La_{0.7}Ca_{0.3}Mn_{0.97}Cu_{0.03}O_3$ perovskite oxides, Inorg. Mater. 38 (2002) 261–264.
[28] L. dos Santos-Gómez, E.R. Losilla, F. Martín, J.R. Ramos-Barrado, D. Marrero-López, Novel microstructural strategies to enhance the electrochemical performance of $La_{0.8}Sr_{0.2}MnO_{3-\delta}$ cathodes, ACS Appl. Mater. Interfaces 7 (2015) 7197–7205.
[29] J. Yang, W.H. Song, Y.Q. Ma, R.L. Zhang, Y.P. Sun, Determination of oxygen stoichiometry in the mixed-valent maganites, J. Magn. Magn. Mater. 285 (2005) 417–421.
[30] S.-B. Lee, T.-H. Lim, R.-H. Soing, D.-R. Shin, S.-K. Dong, Development of a 700 W anode-supported micro-tubular SOFC stack for APU applications, Int. J. Hydrogen Energy 33 (2008) 2330–2336.
[31] J.-H. Kim, R.-H. Song, D.-Y. Chung, S.-H. Hyun, D.-R. Shin, Degradation of cathode current-collecting materials for anode-supported flat-tube solid oxide fuel cell, J. Power Sources 188 (2009) 447–452.
[32] U.-J. Yun, M.-J. Jo, J.-W. Lee, S.-B. Lee, T.-H. Lim, S.-J. Park, R.-H. Song, Operating characteristics of a tubular direct carbon fuel cell based on a general anode support solid oxide fuel cell, Ind. Eng. Chem. Res. 52 (2013) 15466–15471.
[33] G.H.A. Therese, M. Dinamani, P.V. Kamath, Electrochemical synthesis of perovskite oxides, J. Appl. Electrochem 35 (2005) 459–465.
[34] B.-K. Park, R.-H. Song, S.-B. Lee, T.-H. Lim, S.-J. Park, C.-O. Park, J.-W. Lee, Facile synthesis of Ca-doped $LaCoO_3$ perovskite via chemically assisted electrodeposition as a protective film on solid oxide fuel cell interconnects, J. Electrochem. Soc. 163 (2016) F1066–F1071.
[35] N. Saigan, D.G. Ivey, W. Chen, Co/$LaCrO_3$ composite coatings for AISI 430 stainless steel solid oxide fuel cell interconnects, J. Power Sources 185 (2008) 331–337.
[36] Y. Sun, C. Li, W. Zheng, Ionic liquid-assisted hydrothermal synthesis of monoclinic structured $LaVO_4$ nanowires through topotactic transformation from hexagonal $La(OH)_3$ nanowires, Cryst. Growth Des. 10 (2010) 262–267.
[37] L. Wu, Z. Wang, X. Li, H. Guo, L. Li, X. Wang, J. Zheng, Cation-substituted $LiFePO_4$ prepared from the $FeSO_4 \cdot 7H_2O$ waste slag as a potential Li battery cathode material, J. Alloy. Compd. 497 (2010) 278–284.
[38] G. Zampieri, M. Abbate, F. Prado, A. Caneiro, Mn-2p XPS spectra of differently hole-doped Mn perovskites, Solid State Commun. 123 (2002) 81–85.
[39] H. Deng, L. Lin, Y. Sun, C. Pang, J. Zhuang, P. Ouyang, Z. Li, S. Liu, Perovskite-type oxide $LaMnO_3$: an efficient and recyclable heterogeneous catalyst for the wet aerobic oxidation of lignin to aromatic aldehydes, Catal. Lett. 126 (2008) 106–111.
[40] C. Zhang, W. Hua, C. Wang, Y. Guo, Y. Guo, G. Lu, A. Baylet, A. Giroir-Fendler, The effect of A-site substitution by Sr, Mg and Ce on the catalytic performance of $LaMnO_3$ catalysts for the oxidation of vinyl chloride emission, Appl. Catal. B 134–135 (2013) 310–315.
[41] A.G. Bhavani, W.-Y. Kim, J.-S. Lee, Barium substituted lanthanum manganite perovskite for CO_2 reforming of methane, ACS Catal. 3 (2013) 1537–1544.
[42] A.Y. Zuev, D.S. Tsvetkov, Oxygen nonstoichiometry, defect structure and defect-induced expansion of undoped perovskite $LaMnO_{3\pm\delta}$, Solid State Ion. 181 (2010) 557–563.
[43] B.C. Tofield, W.R. Scott, Oxidative nonstoichiometry in perovskites, an experimental survey; the defect structure of an oxidized lanthanum manganite by powder neutron diffraction, J. Solid State Chem. 10 (1974) 183–194.
[44] R. Dudric, A. Vladescu, V. Rednic, M. Neumann, I.G. Deac, R. Tetean, XPS study on $La_{0.67}Ca_{0.33}Mn_{1-x}Co_xO_3$ compounds, J. Mol. Struct. 1073 (2014) 66–70.
[45] L. Zhang, H.Q. He, W.R. Kwek, J. Ma, E.H. Tang, S.P. Jiang, Fabrication and characterization of anode-supported tubular solid-oxide fuel cells by slip casting and dip coating techniques, J. Am. Ceram. Soc. 92 (2009) 302–310.
[46] X. Zhang, B. Lin, Y. Ling, Y. Dong, G. Meng, X. Liu, An anode-supported microtubular solid oxide fuel cell with redox stable composite cathode, Int. J. Hydrogen Energy 35 (2010) 8654–8662.
[47] Y.-H. Heo, J.-W. Lee, S.-B. Lee, T.-H. Lim, S.-J. Park, R.-H. Song, C.-O. Park, D.-R. Shin, Redox-induced performance degradation of anode-supported tubular solid oxide fuel cells, Int. J. Hydrogen Energy 36 (2011) 797–804.
[48] F. Zhao, C. Jin, C. Yang, S. Wang, F. Chen, Fabrication and characterization of anode-supported micro-tubular solid oxide fuel cell based on $BaZr_{0.1}Ce_{0.7}Y_{0.1}Yb_{0.1}O_{3-\delta}$ electrolyte, J. Power Sources 196 (2011) 688–691.
[49] M. Mori, Y. Hiei, N.M. Sammes, G.A. Tompsett, Thermal-expansion behaviors and mechanisms for Ca- or Sr-doped lanthanum manganite perovskites under oxidizing atmospheres, J. Electrochem. Soc. 147 (2000) 1295–1302.
[50] B.-K. Park, J.-W. Lee, S.-B. Lee, T.-H. Lim, S.-J. Park, C.-O. Park, R.-H. Song, Cu- and Ni-doped $Mn_{1.5}Co_{1.5}O_4$ spinel coatings on metallic interconnects for solid oxide fuel cells, Int. J. Hydrogen Energy 38 (2013) 12043–12050.